SANDIA REPORT

SAND2013-8540
Unlimited Release
Printed October 2013

Empirical and Physics Based Mathematical Models of Uranium Hydride Decomposition Kinetics with Quantified Uncertainties

M. Salloum and P.E. Gharagozloo
Sandia National Laboratories, CA

Prepared by
Sandia National Laboratories
Albuquerque, New Mexico 87185 and Livermore, California 94550

Sandia National Laboratories is a multi-program laboratory managed and operated by Sandia Corporation, a wholly owned subsidiary of Lockheed Martin Corporation, for the U.S. Department of Energy's National Nuclear Security Administration under contract DE-AC04-94AL85000.

Approved for public release; further dissemination unlimited.

Sandia National Laboratories

Issued by Sandia National Laboratories, operated for the United States Department of Energy by Sandia Corporation.

NOTICE: This report was prepared as an account of work sponsored by an agency of the United States Government. Neither the United States Government, nor any agency thereof, nor any of their employees, nor any of their contractors, subcontractors, or their employees, make any warranty, express or implied, or assume any legal liability or responsibility for the accuracy, completeness, or usefulness of any information, apparatus, product, or process disclosed, or represent that its use would not infringe privately owned rights. Reference herein to any specific commercial product, process, or service by trade name, trademark, manufacturer, or otherwise, does not necessarily constitute or imply its endorsement, recommendation, or favoring by the United States Government, any agency thereof, or any of their contractors or subcontractors. The views and opinions expressed herein do not necessarily state or reflect those of the United States Government, any agency thereof, or any of their contractors.

Printed in the United States of America. This report has been reproduced directly from the best available copy.

Available to DOE and DOE contractors from
U.S. Department of Energy
Office of Scientific and Technical Information
P.O. Box 62
Oak Ridge, TN 37831

Telephone: (865) 576-8401
Facsimile: (865) 576-5728
E-Mail: reports@adonis.osti.gov
Online ordering: http://www.osti.gov/bridge

Available to the public from
U.S. Department of Commerce
National Technical Information Service
5285 Port Royal Rd
Springfield, VA 22161

Telephone: (800) 553-6847
Facsimile: (703) 605-6900
E-Mail: orders@ntis.fedworld.gov
Online ordering: http://www.ntis.gov/help/ordermethods.asp?loc=7-4-0#online

SAND2013-8540
Unlimited Release
Printed October 2013

Empirical and Physics Based Mathematical Models of Uranium Hydride Decomposition Kinetics with Quantified Uncertainties

Maher Salloum and Patricia. E. Gharagozloo
Sandia National Laboratories, Livermore CA 94550
{mnsallo,peghara}@sandia.gov

Abstract

Metal particle beds have recently become a major technique for hydrogen storage. In order to extract hydrogen from such beds, it is crucial to understand the decomposition kinetics of the metal hydride. We are interested in obtaining a a better understanding of the uranium hydride (UH_3) decomposition kinetics. We first developed an empirical model by fitting data compiled from different experimental studies in the literature and quantified the uncertainty resulting from the scattered data. We found that the decomposition time range predicted by the obtained kinetics was in a good agreement with published experimental results. Secondly, we developed a physics based mathematical model to simulate the rate of hydrogen diffusion in a hydride particle during the decomposition. We used this model to simulate the decomposition of the particles for temperatures ranging from 300K to 1000K while propagating parametric uncertainty and evaluated the kinetics from the results. We compared the kinetics parameters derived from the empirical and physics based models and found that the uncertainty in the kinetics predicted by the physics based model covers the scattered experimental data. Finally, we used the physics-based kinetics parameters to simulate the effects of boundary resistances and powder morphological changes during decomposition in a continuum level model. We found that the species change within the bed occurring during the decomposition accelerates the hydrogen flow by increasing the bed permeability, while the pressure buildup and the thermal barrier forming at the wall significantly impede the hydrogen extraction.

Acknowledgment

The authors would like to acknowledge Andrew Shugard for providing valuable discussions and feedback that were helpful to accomplish this work.

This work was supported by the Advanced Simulation and Computing Physics and Engineering Models (ASC-PEM) programs at Sandia National Laboratories.

Sandia National Laboratories is a multi-program laboratory managed and operated by Sandia Corporation, a wholly owned subsidiary of Lockheed Martin Corporation, for the U.S. Department of Energy's National Nuclear Security Administration under contract DE-AC04-94AL85000.

Contents

Figures

1 Introduction

Hydrogen (H_2) storage in metal hydrides has the potential to store hydrogen safely and stably for long periods of time and release the hydrogen quickly when it is needed [1]. Uranium (U) stores hydrogen at a density of 8.3 atoms per cm^3 of material, higher than most metal hydrides, and at a low equilibrium pressure (less than 0.1 Pa) [2]. Uranium hydride (UH_3) powder beds have been used extensively for hydrogen isotope storage [3–5]. Stored hydrogen isotopes can be recovered by heating the hydride up to temperatures of 400-450^{o}C. Understanding the decomposition kinetics of UH_3 is important for hydrogen storage applications. However, a large amount of variation exists between the few empirical models developed to date [6–9] and no published physics based models are available.

Condon and Larson (1973) [6] studied the reaction kinetics of the U-H system in a high vacuum environment at lower temperatures (60-250^{o}C). The dehydriding reaction was found to be nearly a zero-order reaction with an activation energy of 72.82 kJ/mol. Significant scattering in the measured dehydriding kinetics data was observed due to the existence of oxide contaminants. Stakebake (1979) [7] performed dehydriding experiments at moderate temperatures (200-300^{o}C) and found an activation energy of 39.76 kJ/mol. The discrepancy between the between this value and the one measured by Condon and Larson was attributed to the presence of oxidizing contaminants during Stakebake's experiments. Bloch and Mintz (1981) [8] found a substantial dependence of the UH_3 decomposition kinetics on the surrounding pressure. A plateau pressure, below which decomposition of the UH_3 occurs, was evaluated as a function of temperature. Finally, the recent study of Lindner (1990) [9] resulted in a better understanding of the decomposition mechanism. Through a more thorough experimental study at high temperatures (400-500^{o}C), it was proved that the reaction is controlled by the advance of the U-UH_3 phase such that the reaction fraction can be expressed as:

$$\alpha = 1 - [1 - k(T,P)t]^3 \tag{1}$$

where $k(T,P)$ is the temperature and pressure dependent kinetic coefficient and t is time. Lindner derived a more accurate dependence of k on the temperature and pressure given by:

$$k = k_0 e^{-E_a/RT} \log(P/P_0(T)) \tag{2}$$

where P_0 is the hydrogen plateau pressure as a function of temperature. In a recent multiphysics finite element study [10], oxidation of UH_3 was used to generate a high temperature sufficient to decompose a UH_3 bed. The study relied on decomposition kinetics of Condon and Larson [6] while the UH_3 oxidation kinetics to experimental data [11, 12] without any attempt to improve the decomposition kinetics.

Other empirical models of the U-H reaction have been published [13–16], but did not study the decomposition. A mathematical model of the kinetics of isothermal UH_3 formation under constant near equilibrium pressure was developed by Chernov *et. al.* (2008) [16]. They considered four stages of hydriding: nucleation, skin development, skin growth, and final saturation. The model was then used to fit a series of experimental curves and evaluate the output for the kinetic parameters.

In this work, we derive UH_3 decomposition kinetics in two ways. First, we gather the data obtained from previous experimental studies [6–9] and fit an empirical model of the decomposition kinetics as an Arrhenius dependence on the temperature. Such empirical model is more accurate than the previous individual models since it involves more data and covers a larger temperature range. Second, we develop a physics based model of the UH_3 decomposition that accounts for the hydrogen diffusion and solubility in U. This model enables the computation of the kinetics as a function of temperature. In both models, we quantify the uncertainty in the obtained kinetics using polynomial chaos expansions (PCE). This uncertainty is due to experimental error and limited data. Finally, we apply the computed kinetics to a continuum level model to study the effect of boundary thermal resistance and powder morphological changes in a UH_3 particle bed during decomposition.

2 Polynomial Chaos Expansions

In this section we outline the concept of a PCE. We consider random entities parametrized by a finite collection of real-valued independent and identically distributed (*i.i.d.*) random variables $\xi_1, \ldots, \xi_d$ that share a common distribution function, $\mathcal{P}$. If, for example, ξ is a standard normal random variable on Ω, we write $\xi \sim \mathcal{N}(0,1)$ and $\mathcal{P}_\xi(x) = \frac{1}{\sqrt{2\pi}} e^{-x^2/2}$ is the Probability Density Function (PDF) of ξ. Any random variable admits an expansion of the form:

$$u = \sum_{i=0}^{\infty} u_i \Psi_i(\boldsymbol{\xi}), \tag{3}$$

where the $\{\Psi_i\}_{i=0}^{\infty}$ is an orthogonal basis with respect to the density of $\boldsymbol{\xi} = (\xi_1, \ldots, \xi_d)$ such that,

$$\langle \Psi_i \Psi_j \rangle = \int_\Omega \Psi_i(\boldsymbol{x}) \Psi_j(\boldsymbol{x}) \mathcal{P}_{\boldsymbol{\xi}}(\boldsymbol{x}) d\boldsymbol{x} = \delta_{ij} \langle \Psi_i^2 \rangle \tag{4}$$

where δ_{ij} is the Kronecker delta. The expansion (3) is known as the polynomial chaos expansion (PCE) [17–21] of u. Particularly, in the case where $\xi_m \overset{iid}{\sim} \mathcal{N}(0,1)$, the $\{\Psi_i\}_{i=0}^{\infty}$ are d-variate Hermite polynomials [22]. In practical computations, we approximate $u(\boldsymbol{\xi})$ with a truncated series,

$$u(\boldsymbol{\xi}) \approx \sum_{i=0}^{P} u_i \Psi_i(\boldsymbol{\xi}), \tag{5}$$

where P is finite and depends on the truncation strategy adopted. We consider truncations based on the total degree of the retained polynomials in the series, such that P is a function of the stochastic dimension n and expansion order p according to:

$$P + 1 = \frac{(d+p)!}{d!p!}. \tag{6}$$

Here p refers to the largest polynomial degree in the expansion. One way to derive the PC coefficients of u is by projection on the PC basis following:

$$u_i = \frac{\langle u \Psi_i \rangle}{\langle \Psi_i^2 \rangle}, \qquad k = 0, \ldots, P. \tag{7}$$

This requires numerical evaluation of the projection integrals $\langle u \Psi_i \rangle$ using quadrature rules. This method is referred to as non-intrusive spectral projection (NISP) [21] and will be used in this study. More details about PCEs and their numerical implementations are found in [21].

This page intentionally left blank

3 Chemical Kinetics Experimental Data

3.1 Experimental Data

The measurement of UH_3 decomposition kinetics was the subject of few experimental studies. The kinetics data is reported as either the kinetics Arrhenius pre-exponent or the reaction front speed as a function of temperature and exhibits significant scattering. Figure 1 shows the data gathered from different studies where the units of k were suitably converted to s^{-1}. The empirical fits to the individual data sets exhibit significant discrepancies which induces uncertainty in the overall kinetics coefficient and activation energy. We combine different measured kinetics data in order to cover a bigger temperature range and increase the amount data. Doing so decreases the uncertainty in the fitting parameters of the Arrhenius relationship according to the central limit theorem [23].

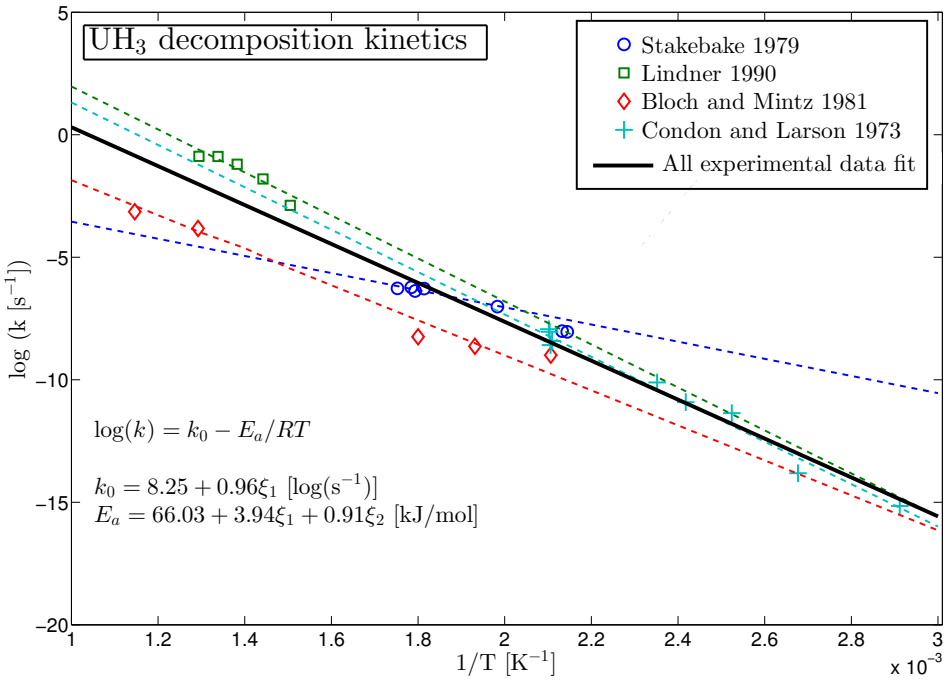

Figure 1. UH_3 decomposition kinetics data gathered from measurement by Condon and Larson [6], Stakebake [7], Bloch and Mintz [8], and Lindner [9]. The dashed lines represent linear fits of the individual data. Also shown are the results of the linear curve fitting of the coefficient k as a function the tempreature T together with their associated uncertainty. ξ_1 and ξ_2 follow standard normal distributions.

Based on this data, we infer according to the method described in [23] an Arrhenius dependence

of the kinetics coefficient as a function of the temperature *i.e.* a linear dependence between $\log(k)$ and $1/T$. This results in two uncertain variables k_0 and E_a that follow normal distributions. ξ_1 characterizes the uncertainty in the $\log(k)$ intercept as $T \to \infty$ and ξ_2 characterizes the uncertainty in the slope of the inferred linear relationship between $\log(k)$ and $1/T$ (see Figure 1). The resulting values of k_0 and E_a are given by:

$$\begin{aligned} \log(k) &= k_0 - E_a/RT \\ k_0 &= 8.25 + 0.96\xi_1 \qquad \left[\log(s^{-1})\right] \\ E_a &= 66.03 + 3.94\xi_1 + 0.91\xi_2 \qquad \left[\text{kJ.mol}^{-1}\right] \end{aligned} \tag{8}$$

3.2 Quantifying Uncertainty in the Decomposition Time

When modeling thermal decomposition of UH_3, a useful quantity of interest is the decomposition time τ *i.e.* the time required to transform a given mass of UH_3 into U. We consider a lumped concentration and temperature model. Such model is suitable to predict the evolution of the concentration in a small quantity of UH_3 as a function of time hence the decomposition time. The U concentration is thus governed by the following ODE [9, 24, 25]:

$$\frac{du}{dt} = 3k(1-u)^{2/3}\log\left(\frac{P_0}{P}\right) \tag{9}$$

where u is the U concentration normalized by the initial UH_3 concentration, k is the kinetics coefficient given as a function of temperature in Eq. 8, P is the local outside pressure and P_0 is the saturation pressure. The term $\log(P_0/P)$ was introduced by Lindner [9] to account for the effect of outside pressure of the decomposition kinetics. According to Eq. 9, it is required that $P < P_0$ for the formation of H_2 gas. P_0 is measured by Lindner [9] as a function of temperature. It is given by:

$$P_0[\text{torr}] = 10^{9.47 - \frac{4700}{T[\text{K}]}} \tag{10}$$

Notice that Eq. 9 does not consider any diffusion taking place in the UH_3 since we assume a lumped mass decomposition given the small amount of UH_3 powder used in the experiments [6, 7, 9]. τ is calculated such that:

$$u(\tau) = 0.999 \tag{11}$$

The kinetics coefficient k involves two uncertain parameters k_0 and E_a (see Eq. 8) leading to an uncertain decomposition time. While different random sampling methods such as Monte Carlo or Latin Hypercube could be used to quantify the uncertainty in τ, we rely on PCEs to represent the uncertainty due to the efficiency and flexibility they offer [21]. We express τ as a PCE of the form:

$$\tau = \sum_{i=0}^{P} \tau_i \Psi_i(\xi_1, \xi_2) \tag{12}$$

We compute the τ_i following Eq. 7 using the NISP scheme, hence we rely on the solution of Eqs. 9 and 11 for given temperature T and pressure P, and for different values of k_0 and E_a sampled on Gauss full quadrature points in the ξ_1 and ξ_2 dimensions. We have $d = 2$ stochastic dimensions. For a reasonable accuracy in the distribution of τ, a convergence study [26] results in an expansion order $p = 4$. Hence, according to Eq. 6, we have $P = 14$. The integral in Eq. 7 is written as the following summation [27]:

$$\tau_i = \frac{1}{\langle \Psi_i^2 \rangle} \sum_{j=1}^{n} \sum_{\ell=1}^{n} \tau\left(\xi_{1,j}, \xi_{2,\ell}\right) w_j w_\ell \qquad \text{for all} \qquad i = 0, \ldots, P \tag{13}$$

Where the location of the ξs and their weights w are given in [21]. The number of such ξs is not straightforward to choose in Monte-Carlo methods since they are slow to converge [21]. However, in PCE methods, this number of quadrature points n per stochastic dimension is chosen such that [27]:

$$n \geq \frac{2p+1}{2}, \tag{14}$$

In order to obtain an exact computation of the integrals in Eq. 7. We therefore choose $n = 5$ resulting in $n^d = 25$ evaluations τ *i.e.* solutions of Eq. 9. Finally, after computing the τ_is, the PDF of τ can be built using Kernel Density Estimation (KDE) [27] after sampling the PCE in Eq. 12. The PCEs were implemented numerically using the UQ toolkit libraries [28]. We plot the PDFs in Figure 2 based on the temperature and pressure used in the experimental studies of by Condon and Larson [6] and Lindner [9]. The PDFs are similar to scew-normal distributions with a tail extending to the high values of τ. Compared to the relative uncertainty in the input parameters k_0 and E_a (see Eq. 8), the resulting uncertainty in τ is significantly bigger due to the nature of the ODE in Eq. 9 known to amplify uncertainty [29]. Decomposition times measured by Condon [6] and Lindner [9] for a given temperature and background pressure fall within the range of the predicted uncertainty as shown in Figure 2.

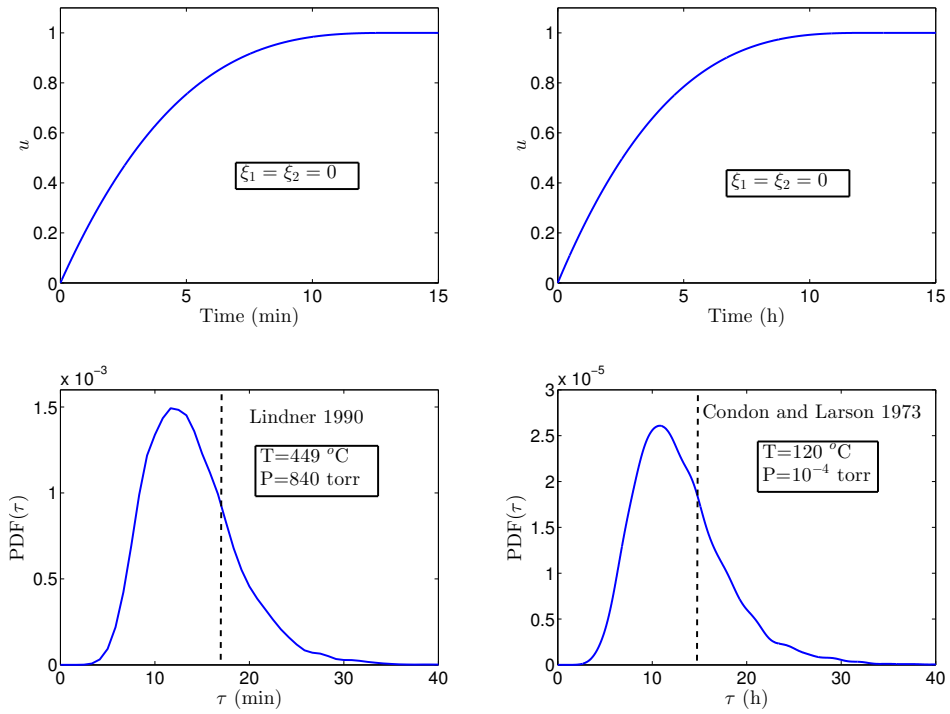

Figure 2. Plots showing: (Top row) the evolution of the non-dimensional concentration u as a function of time for the nominal values of k_0 and E_a, and (bottom row) the PDF of the decomposition time τ generated by propagating the uncertainty in k_0 and E_a in Eq. 9. Also shown is the measured decomposition time in two case studies in the literature [6, 9], as indicated.

4 Mathematical Model Formulation

In this section, we develop a physics based model of the UH_3 decomposition in order to extract the chemical kinetics as a function of temperature. We consider a spherical particle of radius R immersed in a low pressure environment and subjected to a uniform temperature. The UH_3 decomposition is thus initiated at the sphere surface and H_2 molecules diffuse through a U layer from the UH_3-U interface.

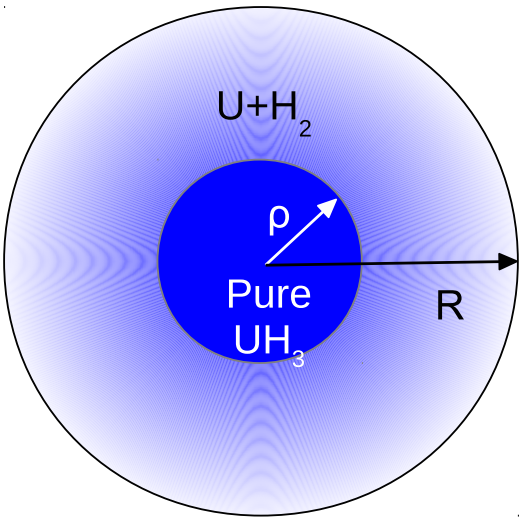

Figure 3. Schematic of the decomposition of a spherical UH_3 particle. The UH_3 decomposes at $r = \rho$ and diffuses within the region $\rho < r < R$. As the decomposition progresses with time, the surface $r = \rho$ moves toward the sphere center.

At a given time, the UH_3 decomposition emanates at the surface $r = \rho$ where the following reaction takes place:

$$UH_3 \rightarrow U + \frac{3}{2}H_2 \tag{15}$$

In other words, the UH_3 molecules dissociate into hydrogen and U molecules. Hence, for $r \leq \rho$, the domain comprises pure UH_3 while for $r > \rho$, the domain comprises hydrogen molecules diffusing in U as shown in Figure 3. As this process evolves with time, the surface $r = \rho$ moves towards the sphere center and controls the UH_3 decomposition [9]. Assuming that this diffusion process is uniform around the sphere, it can be modeled using the following one-dimensional PDE in spherical coordinates:

$$\frac{\partial c}{\partial t} = \frac{1}{r^2}\frac{\partial}{r}\left(r^2 D \frac{\partial c}{\partial r}\right) \qquad \text{in} \qquad r \in [\rho(t), R] \tag{16}$$

where c is the H_2 concentration, t is time, $\rho(t)$ is the radius of the UH_3-U interface. At $r = \rho(t)$, the H_2 concentration is equal to s_{max} the maximum hydrogen solubility in U while at $r = R$, the

H_2 concentration is equal to $s(P,T)$, the hydrogen solubility in U as a function of temperature and outside gas pressure. $s_{max}(T)$ and $s(P,T)$ have been measured as a function of temperature in the experiments of Mallett and Trzeciak [30]. Thus, Eq. 16 is subjected to the following boundary conditions:

$$\begin{aligned} c &= s_{max}(T) \quad \text{at} \quad r = \rho(t) \\ c &= s(P,T) \quad \text{at} \quad r = R \end{aligned} \tag{17}$$

As the decomposition and diffusion progress, the decrease of ρ with time is governed by the following mass conservation equation:

$$-D\frac{\partial c}{\partial r} = \Gamma\frac{\partial \rho}{\partial t} \tag{18}$$

where Γ is the bulk concentration of hydrogen in UH_3 which is much higher than s_{max} [31]. Eq. 18 signifies that the rate of hydrogen decomposing and diffusing in U is equal to the rate at which the UH_3 particle contracts *i.e.* the rate at which ρ decreases with time.

Initially, a thin film of U metal surrounds the UH_3 particle. This film is the result of the hydrogen nucleation at the particle surface. This process is usually modeled by probabilistic models [32]. In previous studies, this initial film thickness was evaluated by fitting the model to experimental data [31]. In this study, we assume that nucleation has already occured and characterize the film thickness by the inital value ρ_0. Thus, the solution of Eq. 16 evaluates the growth of the inital nucleation skin on the UH_3 particle. Nucleation is enhanced with temperature [32] such that ρ_0 is a decreasing function with temperature. More details about the variation of ρ_0 with temperature are found in Section 5. At $t = 0$, the nucleation concentration distribution is given as the following hyperbolic distribution [16, 31]:

$$c = s_{max}(T) - (s_{max}(T) - s(P,T))\frac{R}{r}\frac{r-\rho_0}{R-\rho_0} \tag{19}$$

Using Comsol 4.3 [33], we solve the nonlinear set of equations 16 and 18 subjected to the boundary conditions 17-18 and initial conditions 19, and extract the decomposition kinetics coefficient as:

$$k = -\frac{1}{R\log(P_0/P)}\frac{\partial \rho}{\partial t} \tag{20}$$

where P_0 is given in Eq. 10. It is convenient to divide k by $\log(P_0/P)$ in order to normalize the effect of the outside gas pressure. Details about the solution and model parameters are given in Section 5.

5 Parametric Uncertainty Quantification

The bulk concentration Γ of hydrogen in UH_3 can be estimated by assuming that there is one site per U atom. U forms a lattice with a parameter equal to $a = 0.416$ nm [34] and 6 H atoms in a unit cell. Γ is then $\frac{6}{N_A a^3} = 0.138$ mol.cm^{-3}, where N_A is Avogadro number (6.023×10^{23}mol^{-1}). The particle radius is set to a constant value $R = 0.35\mu$m corresponding to the particle radius obtained in experiments after several hydriding-dehydriding cycles [35]

The published thermophysical properties of the H-U system are limited and exhibit scattering as a function of temperature. For instance, the H_2 solubility and diffusivity in U is reported in previous studies [6, 14, 36–38] as correlations as a function of temperature. All these studies relied on the early raw measurements of Mallett and Trzeciak [30] and Powell *et.al.* [39] plotted in Figure 4. Moreover, the nucleation of H_2 at the UH_3 particle surface is difficult to model and results in an unknown initial film thickness. All these sources of uncertainty result in uncertain predictions of the UH_3 decomposition kinetics. At a given temperature and pressure, the solubility of H_2 in U is given by:

$$s(T,P) = 0.021\exp\left(-42.57[\text{kJ.mol}^{-1}]/RT\right)\sqrt{P[\text{atm}]} \qquad [\text{mol.cm}^{-3}] \tag{21}$$

For $P = 1$ atm, this solubility is plotted as function of temperature in Figure 4 (left, green line).

In this paper, we account for the uncertainty in s_{max} the maximum H_2 solubility in U, D the diffusivity of H_2 in U, and ρ_0/R the initial film thickness. Similar to the method used in Section 3.1, we infer expressions of the pre-exponent and activation energy for D and s_{max} from the data plotted in Figure 4. These expressions are given in Eqs. 22 and 23.

$$\begin{aligned} \log(D) &= D_0 - E_{D,a}/RT \\ D_0 &= -4.13 + 0.316\zeta_1 \qquad \log[\text{cm}^2.\text{s}^{-1}] \\ E_{D,a} &= 45.77 + 2.23\zeta_1 + 0.42\zeta_2 \qquad [\text{kJ.mol}^{-1}] \end{aligned} \tag{22}$$

$$\begin{aligned} \log(s_{max}) &= s_{max,0} - s_{max,a}/RT \\ s_{max,0} &= 0.988 + 0.35\zeta_3 \qquad [\log(\text{mol.cm}^{-3})] \\ s_{max,a} &= 62.99 + 2.21\zeta_3 + 0.82\zeta_4 \qquad [\text{kJ.mol}^{-1}] \end{aligned} \tag{23}$$

where all $\zeta_{i=1\ldots4} \sim \mathcal{N}(0,1)$. As described in Section 4, we assume that ρ_0/R decreases linearly with temperature. The data of Zaika and Rodchenkova [31] suggest that $\rho_0/R = 0.96$ for $T =$

400K. We assume that there is a $p = 2\%$ uncertainty in this value. Thus have:

$$\rho_0/R = 0.96(1 + p\zeta_5) - B(400 - T) \tag{24}$$

Furthermore, we determine B by assuming that at room temperature $T_a = 300$K the initial film thickness is negligible *i.e.* $\rho_0/R = 0.999$ incurring:

$$\rho_0/R = \frac{0.96(1 + p\zeta_5)(T - T_a) + 0.999(400 - T)}{400 - T_a} \tag{25}$$

The assumptions above resulted in five stochastic dimensions that characterize the sources of uncertainty in the particle scale decomposition model of UH_3. We propagate the uncertainties using the NISP scheme similar to Section 3.2. However, since we have a relatively larger number of dimensions we rely on Gauss sparse quadrature points in the $\zeta_{i=1\ldots5}$ dimensions [21] in order to decrease n (see Eq. 13) and alleviate the computational cost of the NISP procedure. Note that the ζs in this section are different than the ξs in Section 3.2 since they characterize different sources of uncertainty. Using the projection equation 7, we derive the PCE for the kinetic coefficient k as a function of temperature as:

$$k(T) = \sum_{i=0}^{P} k_i(T)\Psi_i(\zeta_{i=1\ldots5}) \tag{26}$$

This PCE enables to computation of the standard deviation of k as a function of temperature as follows [21]:

$$\sigma_k(T) = \sum_{i=1}^{P} k_i(T)^2 \langle \Psi_i^2(\zeta_{i=1\ldots5}) \rangle \tag{27}$$

Figure 5 shows the computed kinetics coefficient k (thick blue line) plotted as a function of $1/T$ together with its associated uncertainty level ($\pm 3\sigma_k(T)$). The computed kinetics is in agreement with the measured values found in the literature. The computed mean activation energy is higher than the measured value probably due to the assumptions introduced in the particle model. For instance, there are uncertainties about the shape of the UH_3 particles, their size and their shrinking process upon decomposition. These phenomena are not captured in the model. Moreover, the one-dimensional assumption on the hydrogen diffusion in uranium might not be a good approximation. Nevertheless, the uncertainty quantified in the model covers the scattering in the measured values mainly for moderate and low decomposition temperatures that are preferred in practice.

Unlike the empirical model developed in Section 3, this model can be further detailed to account for other uncertainties and physical phenomena occurring during the decomposition such as the particle size and shape, the existence of contaminants, etc. Additionally, the mathematical model alleviates the burden of expensive experiments.

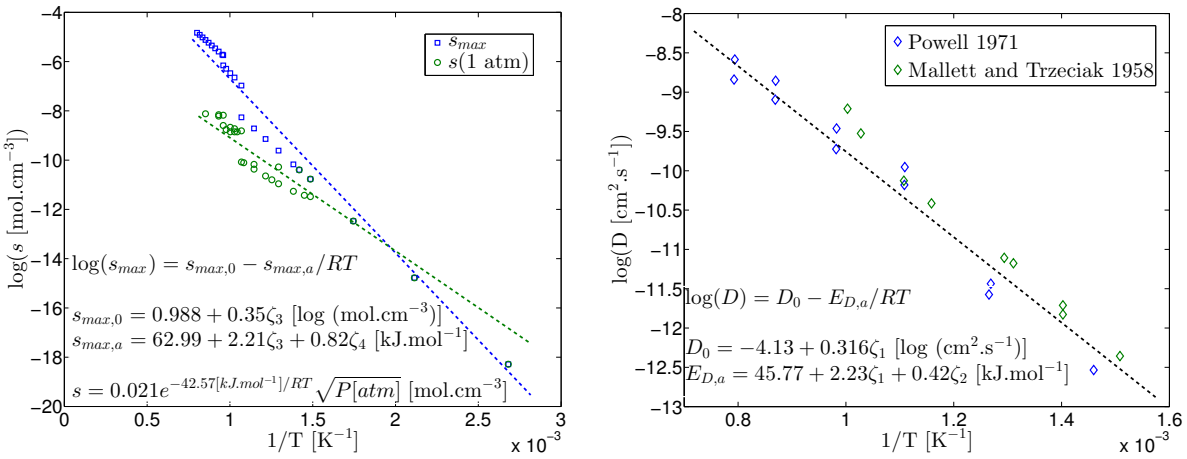

Figure 4. Plots showing raw experimental data as a function of temperature of the (left) H_2 solubility in U measured by Mallett and Trzeciak [30], and (right) H_2 diffusivity in U measured by Mallett and Trzeciak [30] and Powell *et.al.* [39], as indicated. The dashed lines denote linear best fits of the parameters.

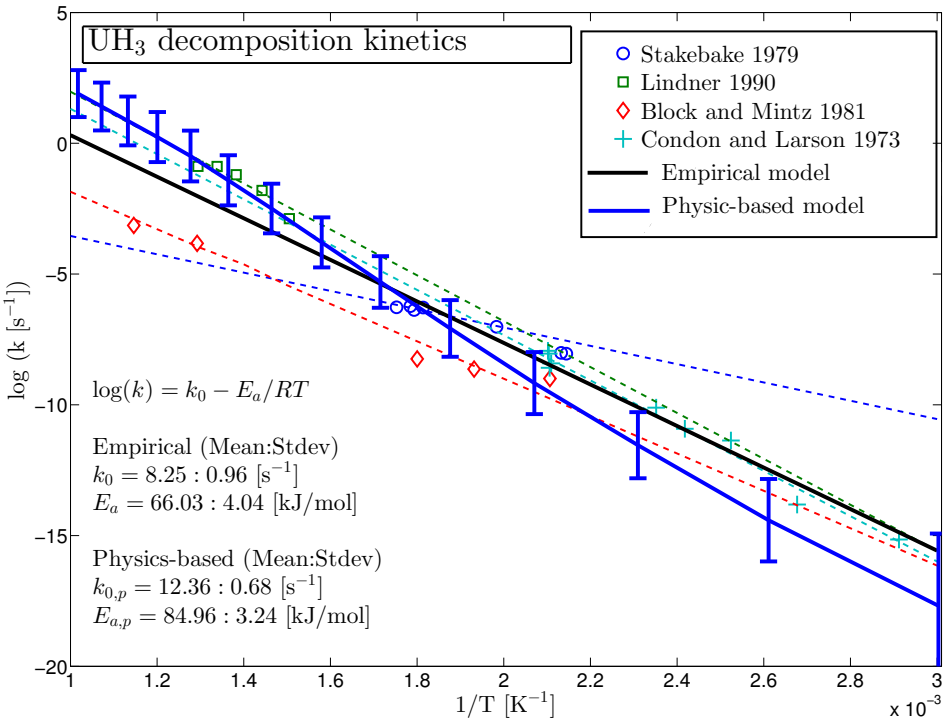

Figure 5. Plot showing the same UH_3 decomposition kinetics values in Figure 1 as well as the kinetics predicted by the particle model. Also shown are the error bars ($\pm 3\sigma_k(T)$) calculated by propagating the parametric uncertainty in the model. Results are generated for a UH_3 particle size, $R = 0.35\mu$m and an outside pressure of 10^{-5} Torr.

6 Continuum Model

In this section, we develop a continuum scale numerical model of UH_3 powder decomposition. The model aims to understand the different physical phenomena involved in the process, such as the pressure buildup in the powder bed, the bed permeability, the morphological changes in the bed, etc., and their effects on the H_2 extraction rate. The model relies on the decomposition kinetics extracted from the physics-based model in Section 4 and comprises the governing equations for momentum, energy and mass transport, and the chemical reactions [10]. Unless otherwise stated, the units of the variables are CGS.

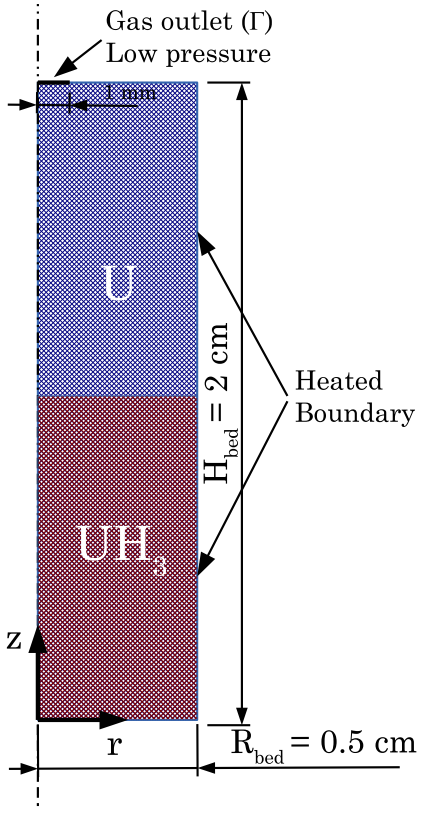

Figure 6. A schematic showing the axisymmetric reactor where UH_3 is decomposing. The H_2 leaves the reactor at the cylinder upper surface where a low pressure is imposed. The heat is provided to the UH_3 bed by either imposing a temperature in the whole domain or by setting a temperature at the right wall as indicated.

We consider the closed axisymmetric bed illustrated in Figure 6. The bed is filled with a mass m of UH_3 powder giving an initial porosity:

$$\phi_0 = 1 - \frac{m}{\rho_{UH_3} V_{bed}} \tag{28}$$

where $\rho_{UH_3} = 10.95 \text{g.cm}^{-3}$ is the density of the solid UH_3 and V_{bed} =1.571 cm^3 is the total bed volume. There is an opening at the upper boundary of the bed where the H_2 gas is extracted by imposing a low suction pressure. We assume that heat is supplied to the bed in two different ways. First, we consider that the whole bed is uniformly heated to a given temperature. In this case, the temperature is constant throughout the bed for the whole simulation time, thus the energy heat conduction equation is not solved. Secondly, we assume that the right boundary is set to a given temperature such that heat can be conducted to the bed. In the second case, we consider the situation where a thermal barrier forms on the bed wall due to the shrinkage of the solid particles upon the species change from UH_3 to U. In both cases we account for the variability of the porosity in the bed also due to species change.

6.1 Governing Equations

The consumption (*resp.* production) of UH_3 (*resp.* U) is governed by the following chemical reaction:

$$UH_3 \rightarrow U + \frac{3}{2}H_2 \tag{29}$$

The production of U is described by the conservation equation:

$$\frac{d[U]}{dt} = R_{UH_3} \tag{30}$$

where the transport of these two species either by diffusion or mechanical deformation is neglected. Eq 30 is the dimensional form of Eq. 9. Thus R_{UH_3} is given by:

$$R_{UH_3} = 3k\left([UH_3]_0 - [U]\right)^{2/3}[UH_3]_0^{1/3}\log\left(\frac{P_0}{P}\right) \tag{31}$$

where $[UH_3]_0$ is the initial molar concentration of UH_3 in the reactor bed, P is local pressure and P_0 is given by Eq. 10.

Modeling the release of H_2 from the bed requires an equation describing momentum transport. The porous bed provides a substantial restriction to gas flow. Many different forms of equations have been developed for describing flow through porous media [40, 41]. In our case, the flow is laminar with a Reynolds number of about 0.02, hence the flowing gas inertia is neglected. Given the large size of the porous UH_3 bed compared to the pore size, we neglect the domain boundary effects. Under these assumptions, Darcy's law appropriately simulates the flow of the H_2 gas in the UH_3 bed [42]. Darcy's equation is given by:

$$\frac{\partial(\rho\phi)}{\partial t} - \nabla\cdot\left(\frac{\kappa\rho}{\mu}\nabla P\right) = \frac{3}{2}R_{UH_3}M_{H_2} \tag{32}$$

where ρ and μ are the H_2 gas density and dynamic viscosity, respectively, P is the gas pressure, and ϕ and κ are the bed porosity and permeability, respectively (see Section 6.2). The gas density ρ_{gas} is related to its pressure by the ideal gas law:

$$\rho = \frac{PM_{H_2}}{\mathcal{R}T} \tag{33}$$

where $\mathcal{R} = 8.314$ J.mol^{-1}.K^{-1} is the ideal gas constant. The source term $\frac{3}{2}R_{UH_3}$ on the right-hand side of the equation accounts for the production of H_2 gas phase within the UH_3 bed.

When a constant temperature at the bed lateral surface, heat transfer occurs by both convection and conduction. Within the porous medium, the gas and solid phases are assumed to have the same temperature at any given point and time. The following heat conduction-convection equation describes the heat transfer:

$$(\rho c_p)_{bed} \frac{\partial T}{\partial t} + (\rho c_p)_{gas} \boldsymbol{V} \cdot \boldsymbol{\nabla} T = \nabla \cdot (k_{bed} \boldsymbol{\nabla} T) - R_{UH_3} \Delta H_{UH_3} \tag{34}$$

where T is the temperature, $\boldsymbol{V}$ is the gas velocity vector, k_{bed} =0.01 W.cm^{-1}.K^{-1} is the effective thermal conductivity and ΔH_{UH_3} = 128 kJ.mol^{-1} (endothermic) [38, 43, 44] is the enthalpy of decomposition of UH_3. Note that the second term on the left-hand side describing convection uses the density and specific heat of the gas because it is the phase that is in motion. The thermal inertia term (first term on left-hand side) and the conduction term (first term on right-hand side) use the properties of the solid phase because they are much larger than the corresponding gas phase values [10]. The source term accounts for heat absorbed by the UH_3 bed in order to produce the H_2 gas which transport occurs by convection and diffusion, as described by [45]:

$$\frac{\partial (c\phi)}{\partial t} + \nabla \cdot (c\boldsymbol{V}) = \nabla \cdot (\mathcal{D}^* \boldsymbol{\nabla} c) + \frac{3}{2} R_{UH_3} \tag{35}$$

where c is the molar concentration of H_2, $\mathcal{D}^*$ is the effective diffusivity of H_2. Note that the convection term is in conservative form *i.e.*, the divergence operator acts on the product of concentration and velocity, which is necessary due to the variability of the total gas density.

6.2 Bed Hydraulic Properties

The effective diffusivity of H_2 accounts for the solid particles existing in the gas stream, it is given by [46, 47]:

$$\mathcal{D}^* = \frac{D_{H_2}}{\theta} \tag{36}$$

where θ is the bed tortuosity calculated by the following correlation [35]:

$$\theta = \frac{1.25}{\phi^{1.1}} \tag{37}$$

Contraction is known to occur upon the UH_3 decomposition since the powder particle shrink due to the difference in density between UH_3 and U. Thus the porosity varies within the bed as the reaction progresses. Its local value is calculated by:

$$\phi = 1 - \frac{([UH_3]_0 - [U]) M_{UH_3}}{\rho_{UH_3}} - \frac{[U] M_U}{\rho_U} \tag{38}$$

The local bed permeability is calculated using the Young formula [10, 48]:

$$\kappa = \frac{\phi d_p^2}{\theta^2}\left(\frac{1}{32} + \frac{5}{12}Kn\right), \tag{39}$$

where d_p is the characteristic pore size estimated as a function of the particle radius R and porosity ϕ using geometric considerations on the pore-particle structure as [46]:

$$d_p = R\left\{\left[\frac{3(1-\phi)}{8\pi}\right]^{-1/3} - 2\right\} \tag{40}$$

The Knudsen number $Kn = \lambda/d_p$ is the ratio between the gas mean free path, λ, and the characteristic pore size. The mean free path is given by:

$$\lambda = \frac{\mathcal{R}T}{\pi\sqrt{2}N_A P d_{H_2}^2} \tag{41}$$

where $N_A = 6.023 \times 10^{23}\text{mol}^{-1}$ is Avogadro's number and $d_{H_2} = 6.2 \times 10^{-9}$ cm is the H_2 molecule diameter.

6.3 Initial and Boundary Conditions

The bed is axisymmetric therefore at $r = 0$ we have:

$$\frac{\partial T}{\partial r} = \frac{\partial P}{\partial r} = \frac{\partial c}{\partial r} = \frac{\partial u_r}{\partial r} = \frac{\partial u_z}{\partial r} = 0 \tag{42}$$

The other boundaries are rigid walls except a 1 mm opening at $r = 0$ to extract the H_2 gas (see Figure 6) where we impose a low pressure $P_{outlet} = P_{init} = 10^{-5}$[Torr]. As mentioned in the beginning of this section, we consider two scenarios of the bed decomposition. When the temperature is held constant throughout the bed, Eq. 34 is not solved. In the other case, the bed is heated at its lateral wall where a temperature T_{wall} is imposed. In the situation where a thermal barrier forms on this wall, we assume a convection boundary condition such that the convection coefficient h is given by:

$$h = \frac{k_{H_2}}{g} \tag{43}$$

where k_{H_2} is the H_2 thermal conductivity and g is the barrier thickness assumed to be uniform along the bed and which can be computed as a function of the mean bed porosity as:

$$g = R_{bed}\left(1 - \sqrt{\frac{\phi_0}{\bar{\phi}}}\right) \tag{44}$$

where R_{bed} is the bed radius, ϕ_0 is the initial bed porosity given in Eq. 28 and $\bar{\phi}$ is the mean porosity in the bed.

The bed is initially contains pure UH_3 powder at low pressure therefore at $t = 0$ we have:

$$\begin{aligned} [U] &= 0 \\ T &= T_{init} \\ P_{init} &= 10^{-5} \quad \text{[Torr]} \\ c_{init} &= \frac{P_{init}}{\mathcal{R} T_{init}} \end{aligned} \tag{45}$$

Remark Note that we do not explicitly model the free gas flow in this barrier, we assume that the hydraulic effect of this barrier is taken into account by the increase in the porosity reflected in Eq. 38.

This page intentionally left blank

7 Results

Eqs. 30, 32, 34 and 35 were simulated in Comsol 4.3 [33]. When the temperature is assumed to be uniformed through the bed, Eq. 34 is excluded from the model. For such cases, the computed H_2 flow rates at the bed outlet are plotted in Figure 7. The time corresponding to a sudden drop and/or a discontinuity in the flow rate signifies the time required to decompose the whole bed. This time is substantially high for moderate temperatures ($\sim$ 3 hours). This is mainly attributed to the hydraulic resistance of the bed and the local pressure buildup that slows down the kinetics. Figure 7 also shows the effect of the particle shrinkage which results in local porosity and permeability increase within the bed. The increase in the average porosity is plotted in Figure 10 (top) for different temperatures. A maximum porosity of about 0.74 is reached at the end of the decomposition. The overal bed hydraulic resistance is decreased leading to an increase in the H_2 extraction rate and a three-fold decrease in the decomposition time. Therefore, such morphological changes in the bed are important and should be accounted when modeling reactive flows with species change in porous beds.

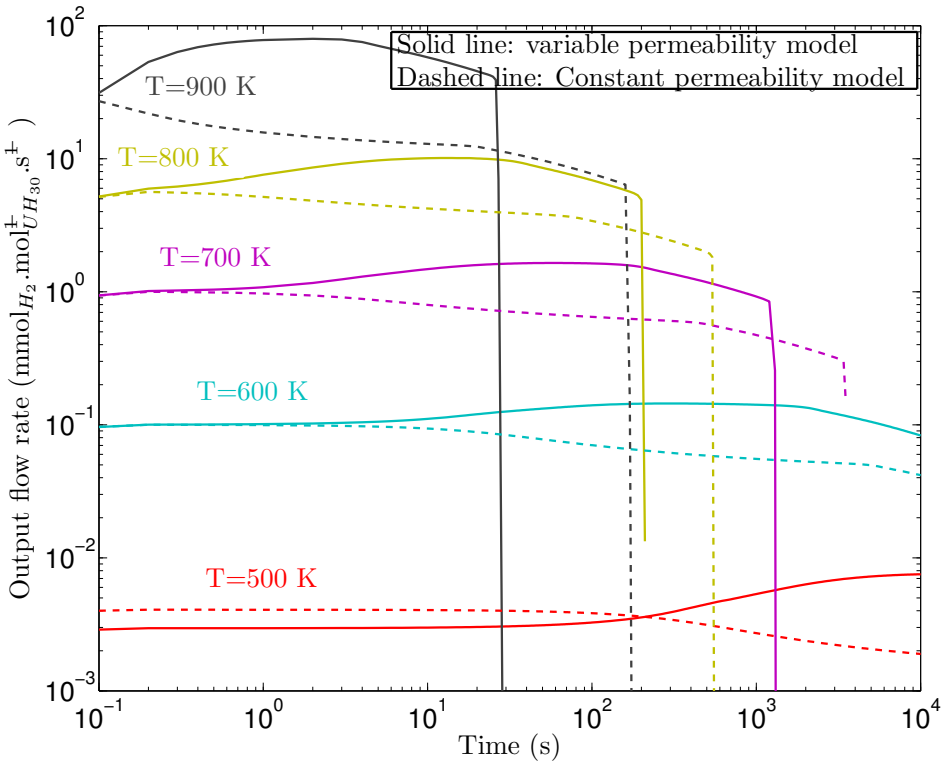

Figure 7. Plots showing the H_2 flow rate as a function of time at the bed outlet for different temperatures assumed to be constant throughout the bed. The flow rate is normalized by the initial number of UH_3 moles. Results are generated when the particle shrinkage is accounted for in the simulations (solid lines) and when it is neglected (dashed line), as indicated.

Figure 8 shows snapshots of the H_2 gas velocity and pressure and the reaction rate for a uniform bed temperature $T = 800$K at $t = 60$s. At this time, approximately one half of the bed is reacted where the upper part is fully transformed into a porous phase U. Despite the increasing permeability in this phase induced by the particle shrinkage, the pressure increases in this upstream UH_3 phase causing a significant decrease in the reaction kinetics according to Eq. 31.

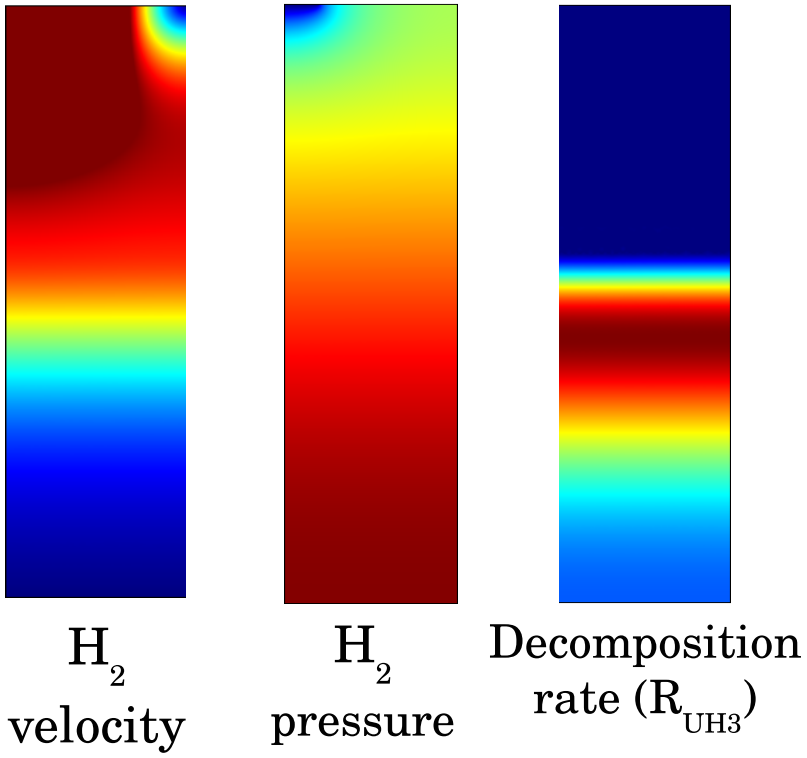

Figure 8. Plots showing: (left) the H_2 gas velocity in cm.s^{-1}, (middle) the H_2 gas pressure in Torr, and (right) the reaction kinetics R_{UH_3} in s^{-1}. Results are generated for a uniform bed temperature $T = 800$K at $t = 60$s where the bed porosity and permeability are assumed to vary locally with the bed phase.

When the bed is heated by imposing a temperature at its vertical wall, the decomposition time is higher than in the case of a constant temperature bed since the heat must conduct into the bed as shown in Figure 9. In this case, we study the formation of a thermal barrier at the bed wall during the decomposition due to the particle shrinkage. The change in average porosity in this case is plotted in Figure 10 (bottom). The thermal barrier impedes the heat transport to the UH_3 particles and substantially increases the decomposition time especially at high temperatures.

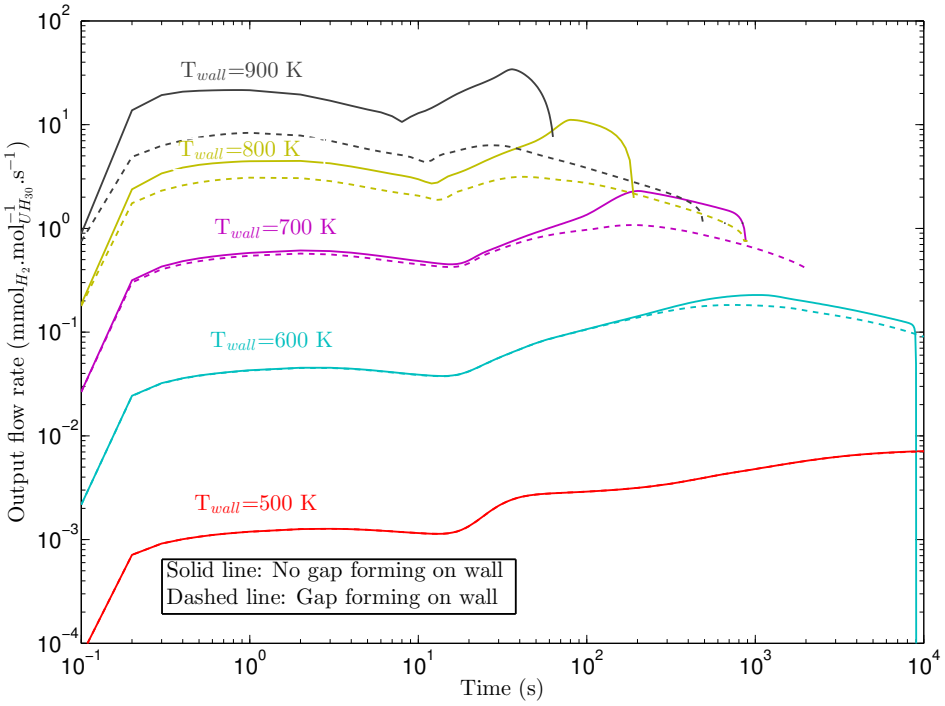

Figure 9. Plots showing the H_2 flow rate as a function of time at the bed outlet for different wall temperatures. The flow rate is normalized by the initial number of UH_3 moles and the particle shrinkage is accounted for in the simulations. Results are generated when the thermal barrier forming at the wall is accounted for in the simulations (dashed lines) and when it is neglected (solid line), as indicated.

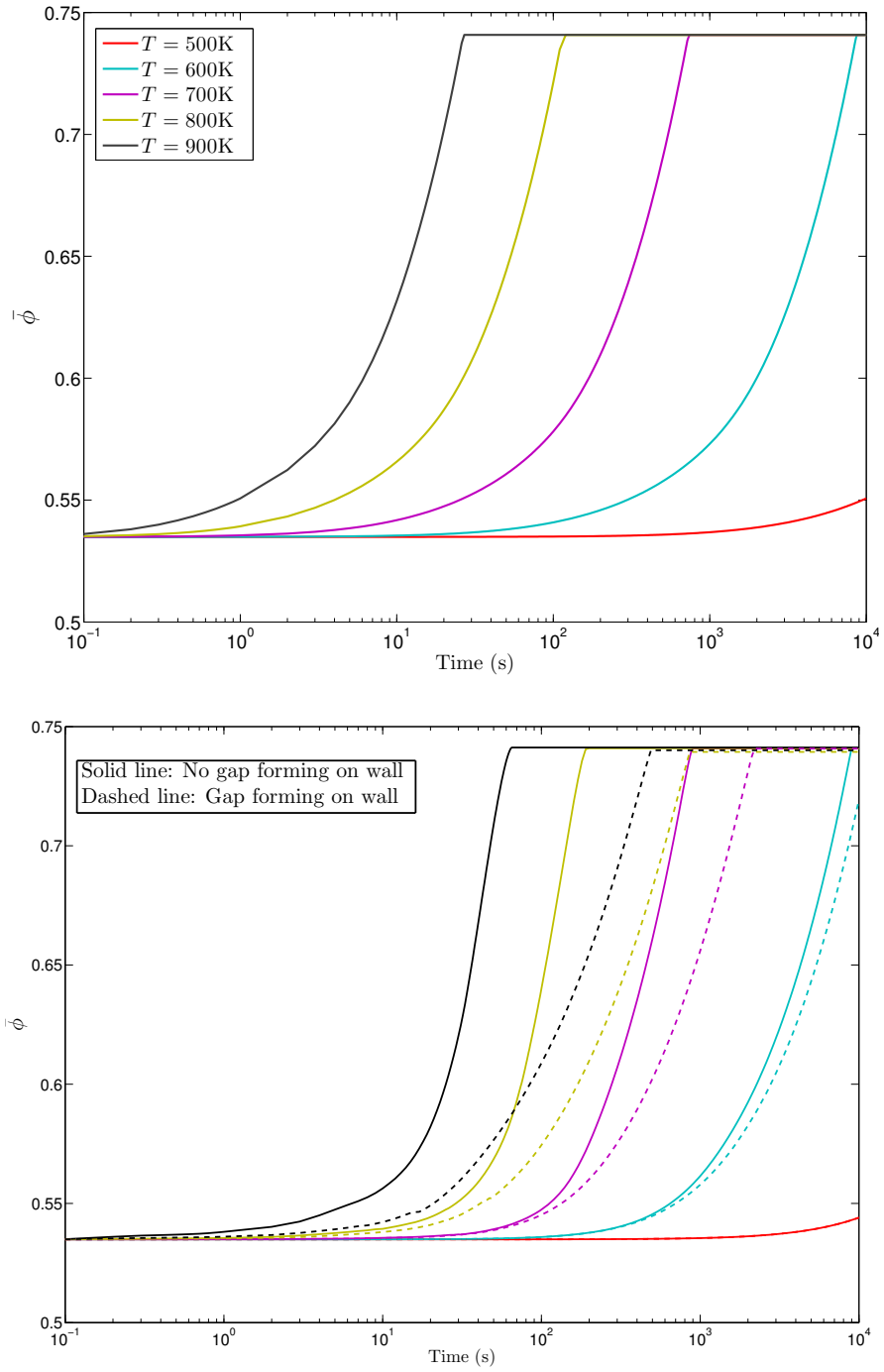

Figure 10. Plots showing the average porosity change during the UH_3 bed decomposition for different temperatures.The particle shrinkage is accounted for in the simulations. Results are generated for: (top) constant temperature bed, and (bottom) wall heated bed where when the thermal barrier forming at the wall is accounted for in the simulations (dashed lines) and when it is neglected (solid line), as indicated.

8 Conclusion

In this paper, we developed an empirical model and a physics based model of the uranium hydride decomposition kinetics. The empirical model is based on measured kinetics values found in the literature. This model was used to predict the decomposition time of a lumped mass of uranium hydride together with its associated uncertainty resulting from the scattering in the experimental data. Measured decomposition times were found to fall in the range of the predicted uncertainty.

Given that different physical phenomena can influence the decomposition kinetics, we developed a physics based model to evaluate the kinetics by simulating the hydrogen release from a uranium hydride particle while accounting for the uncertainty in the hydrogen diffusivity and solubility in uranium. This model predicted kinetics comparable with measured values in the literature while the quantified uncertainty covered the scattering found in the experiments at low and moderate temperatures which are the operating temperatures often used in practice. This model alleviates the cost and complications of experimental studies and it can be further detailed to study the effects of particle size and shape, gas contaminants, etc., on the decomposition kinetics.

We finally developed a continuum multiphysics model of the uranium hydride decomposition. The model explicitly considers the reaction rate computed in the physics-based particle model, heat transport, and mass transport within a cylindrical bed. We considered two cases of the decomposition. First we assumed that the heat is supplied by uniformly imposing a uniform temperature throughout the bed. In this case, we showed that it is crucial to account for the change in the local bed porosity which results from the species change upon decomposition. These morphological changes lead to a ten-fold increase in the bed permeability. Secondly, we considered the case where the bed is heated at its lateral wall surface. In this case, we showed that a significant delay in the bed decomposition would result if a thermal barrier forms at the wall. In both cases, the decomposition times are relatively high for lower and moderate temperatures mainly due to the hydraulic resistance of the porous uranium phase and due to the pressure buildup in the unreacted regions. It is clear from these results that alterations on the bed geometry and properties should be employed to decrease the decomposition time. For example, channels can be drawn inside the bed to decrease the overall bed resistance thereby accelerating the hydrogen extraction. The continuum model developed in this paper could be easily and quickly used to test such modifications.

Although the present physics based particle and continuum model development and findings appear promising, additional research is needed to further strengthen the underlying methodology, to extend its scope, and address remaining unknowns. For example, uncertainties in the particle size and shape should be accounted for in the particle model along with the effects of contaminants on the resulting decomposition kinetics.

9 References

[1] R. Wiswall. Hydrogen storage in metals. In *Topics in Applied Physics*. Springer, 1978. 7

[2] R.D. Kolasinski, A.D. Shugard, C.R. Tewell, and D.F. Cowgill. Uranium for hydrogen storage applications: A materials science perspective. Report SAND2010-5195, Sandia National Laboratories, 2010. 7

[3] C.C. Bowman and V.A. Vis. Tritium handling facility at KMS fusion inc. *J. Vac. Sci. Tech. A: Vacuum, Surfaces, and Films*, 8(3):2890, 1990. 7

[4] L.K. Heung. Tritium transport vessel using depleted uranium. *Fusion. Tech.*, 28(3):1385, 1995. 7

[5] T. Hayashi *et.al.* Safe handling experience of a tritium storage bed. *Fusion. Eng. Des.*, 83:1429, 2008. 7

[6] J.B. Condon and E.A. Larson. Kinetics of the uranium-hydrogen system. *J. Chem. Phys.*, 59:855, 1973. 7, 8, 11, 12, 13, 14, 17

[7] J.L. Stakebake. Kinetics for the reaction of hydrogen with uranium powder. *J. Electrochem. Soc.*, 126(9):1596–1601, 1979. 7, 8, 11, 12

[8] J. Bloch and M.H. Mintz. Kinetics and mechanism of the U-H reaction. *J. Less. Common. Metals.*, 81:301–320, 1981. 7, 8, 11

[9] D.L. Lindner. Isothermal decomposition of uranium hydride. *J. Less. Comm. Metals.*, 157:139, 1990. 7, 8, 11, 12, 13, 14, 15

[10] M.P Kanouff, P.E. Gharagozloo, M. Salloum, and A.D. Shugard. A multiphysics numerical model of oxidation and decomposition in a uranium hydride bed. *Chem. Eng. Sci.*, 91:212–225, 2013. 7, 21, 23, 24

[11] M. Salloum, M.P. Kanouff, A.D. Shugard, and P.E. Gharagozloo. A coupled transport and solid mechanics formulation for modeling oxidation and decomposition in a uranium hydride bed. In *International Mechanical Engineering Congress and Exposition., Paper No: IMECE2012- 87174*, November 2012. 7

[12] M. Salloum, A.D. Shugard, M.P. Kanouff, and P.E. Gharagozloo. A coupled transport and solid mechanics formulation with improved reaction kinetics parameters for modeling oxidation and decomposition in a uranium hydride bed. Report SAND2013-2001, Sandia National Laboratories, 2013. 7

[13] J.B. Condon. Nucleation and growth in the hydriding reaction of uranium. *J. Less. Common. Metals.*, 73:105–112, 1980. 7

[14] J.R. Kirkpatrick. Diffusion with chemical reaction and a moving boundary. *J. Phys. Chem.*, 85:3444–3448, 1981. 7, 17

[15] G.L. Powell, W.L. Harper, and J.R. Kirkpatrick. The kinetics of the hydriding of uranium metal. In *International Symposium on Metal-Hydrogen Systems, Fundamentals and Applications*. Elsevier Science Sa Lausanne, 1990. 7

[16] I.A. Chernov, J. Bloch, and I.E. Gabis. Mathematical modelling of UH_3 formation. *Int. J. Hyd. Ener.*, 33:5589–5595, 2008. 7, 16

[17] S. Wiener. The Homogeneous Chaos. *J. Comp. Phys.*, 224:560–586, 2007. 9

[18] R.H. Cameron and W.T. Martin. The orthogonal development of nonlinear functionals in series of Fourier-Hermite functionals. *Ann. Math.*, 48:385–392, 1947. 9

[19] S. Janson. *Gaussian Hilbert Spaces*. Cambridge University Press, 1997. 9

[20] R.G. Ghanem and P.D. Spanos. *Stochastic Finite Elements: A Spectral Approach*. Springer Verlag, 1991. 9

[21] O.P. Le Maître and O.M. Knio. *Spectral Methods for Uncertainty Quantification with Applications to Computational Fluid Dynamics*. Springer, 2010. 9, 12, 13, 18

[22] M. Abramowitz and I.A. Stegun. *Handbook of Mathematical Functions*. Dover, 1970. 9

[23] M. Salloum, K. Sargsyan, H.N. Najm, B. Debusschere, R. Jones, and H. Adalsteinsson. A stochastic multiscale coupling scheme to account for sampling noise in atomistic-to-continuum simulations. *SIAM. Multi. Model. Simu.*, 10(2):550–584, 2011. 11

[24] J.R. Kirkpatrick, N.S. Mackay, and P.D. Wheatly. Review of uranium hydriding and dehydriding rate models in goth-snf for spent fuel MCO calculations. Internal report, Idaho National Engineering and Environmental Laboratory, 2003. 12

[25] A. Khawam and D.R. Flanagan. Solid-state kinetic models: Basics and mathematical fundamentals. *J. Phys. Chem. B.*, 110(35):17315–17328, 2006. 12

[26] O.P. Le Maître, M.T. Reagan, H.N. Najm, R.G. Ghanem, and O.M. Knio. A stochastic projection method for fluid flow. II. Random process. *Journal of Computational Physics*, 181:9–44, 2002. 13

[27] F. Rizzi, H.N. Najm, B.J. Debusschere, K. Sargsyan, M. Salloum, H. Adalsteinsson, and O.M. Knio. Uncertainty quantification in md simulations. part i: Forward propagation. *SIAM Mult. Modell. Simu.*, 10(4):1428–1459, 2012. 13

[28] The uncertainty quantification (UQ) toolkit. http://www.sandia.gov/uqtoolkit/, Sandia National Laboratories, 2011. 13

[29] M.T. Reagan, H.N. Najm, R.G. Ghanem, and O.M. Knio. Uncertainty quantification in reacting flow simulations through non-intrusive spectral projection. *Combustion and Flame*, 132:545–555, 2003. 13

[30] M.W. Mallett and M.J. Trzeciak. Hydrogen-uranium relationships. *Trans. ASM*, 50:981–989, 1958. 16, 17, 19

[31] Y.V. Zaika and N.I. Rodchenkova. Boundary-value problem with moving bounds and dynamic boundary conditions: Diffusion peak of tds-spectrum of dehydriding. *App. Math. Modelling.*, 33:3776–3791, 2009. 16, 17

[32] M.E. Brown, D. Dollimore, and A.K. Galwey. Comprehensive chemical kinetics. volume 22. Elsevier: Amsterdam, 1980. 16

[33] *Comsol Multiphysics 43: User's Guide*. Comsol, 2012. 16, 27

[34] C.D. Taylor, T. Lookman, and R.S. Lillard. Ab-initio calculations of the uranium-hydrogen system: Thermodynamics, hydrogen saturation of α-u and phase-transformation to UH_3. *Acta. Mater.*, 58:1045–1055, 2010. 17

[35] A.D. Shugard, G.M. Buffleben, T.A. Johnson, and D.B. Robinson. Isotope exchange between gaseous hydrogen and uranium hydride powder. *J. Nucl. Mater.*, 2013. accepted. 17, 23

[36] W.M. Mueller. *Metal Hydrides*. Academic Press, New York, 1968. 17

[37] J.R. Kirkpatrick and J.B. Condon. The linear solution for hydriding of uranium. *J. Less. Common. Metals.*, 172-174:124–135, 1991. 17

[38] F. Manchester and A. San-Martin. The H-U (hydrogen-uranium) system. *J. Phase. Equil.*, 16:263, 1995. 17, 23

[39] G.L. Powell, J.B. Condon, and R.A. Strehlow. An instrument for the determination of hydrogen in metals. Internal report, Oak Ridge Y-12 Plant, 1971. 17, 19

[40] K. Vafai. *Handbook of Porous Media*. Taylor & Francis, 2005. 22

[41] E.A. Mason and A.P. Malinauskas. Gas transport in porous media: The dusty gas model. In *Chemical Engineering Monographs*. Elsevier, 1983. 22

[42] A.-R.A. Khaled and K. Vafai. The role of porous media in modeling flow and heat transfer in biological tissues. *Int. J. Heat. Mass. Trans.*, 46:4989–5003, 2003. 22

[43] B.M. Abraham and H.E. Flotow. The heats of formation of uranium hydride, uranium deuteride and uranium tritide at 25^{o}C. *J. Am. Chem. Soc.*, 77(6):14461448, 1955. 23

[44] D.R. Lide. CRC handbook of chemistry and physics. CRC Press, 2004. 23

[45] R.B. Bird, W.E. Stewart, and E.N. Lightfoot. *Transport Phenomena*. Wiley & Sons, Inc., 1960. 23

[46] F.A.L. Dullien. *Porous Media: Fluid Transport and Pore Structure*. Academic Press., 1979. 23, 24

[47] D.M. Ruthven. *Principles of Adsorption and Adsorption Processes*. Wiley Interscience., 1984. 23

[48] J.B. Young and B. Todd. Modelling of multi-component gas flows in capillaries and porous solids. *Int. J. Heat. Mass. Trans.*, 48:5338, 2005. 24

DISTRIBUTION:

1	Technical Library, 08944 (electronic)	MS 0899
1	Paul Spence, 8254	MS 9035
1	Michael L. Chiesa, 8259	MS 9042
1	Maher Salloum, 08961	MS 9158
1	Andrew D. Shugard, 8254	MS 9661
1	Patricia E. Gharagozloo, 08365	MS 9957
1	Greg Wagner, 08365	MS 9957

Sandia National Laboratories